Journal of Computational Physics **158,** 28–50 (2000)
doi:10.1006/jcph.1999.6404, available online at http://www.idealibrary.com on IDEAL®

A Representation of Bounded Viscous Flow Based on Hodge Decomposition of Wall Impulse

D. M. Summers

School of Mathematical and Physical Sciences, Napier University, 219 Colinton Road, Edinburgh EH14 1DJ, Scotland
E-mail: davids@maths.napier.ac.uk

Received December 17, 1998; revised October 29, 1999

A Lagrangian representation of bounded incompressible flow is introduced in which viscous boundary conditions are given kinematic expression by the generation of impulse at the wall. The relationship between such a process and the boundary conditions is deduced from two complementary Hodge decompositions. The orientation of the created impulse vector may be chosen to be parallel at the wall (this being equivalent to a thin vortex doublet sheet) or normal at the wall (this being a thin monopole vortex sheet). Although the representation is developed here for two dimensions, it can be generalized in a natural way to three dimensions. The case of tangentially oriented wall impulse is applied to flow over a semi-infinite plate; the case of normally oriented wall impulse is applied to flow past a circular cylinder.

Key Words: fluid impulse; vortex methods; viscous flow.

1. INTRODUCTION

The problem of modeling slightly viscous flow over a solid boundary, $\partial\mathcal{D}$, may be formulated in terms of vorticity transport (expressed here for two dimensions),

$$\frac{D\boldsymbol{\xi}}{Dt} = \frac{1}{Re}\Delta\boldsymbol{\xi} \tag{1}$$

where D/Dt is the material derivative, Re is Reynolds number, and Δ is the Laplacian operator. The vorticity field, $\boldsymbol{\xi}$, is defined as the curl of the velocity field $\mathbf{u}$, namely $\boldsymbol{\xi} = \nabla \times \mathbf{u}$. We consider the flow to be incompressible ($\nabla \cdot \mathbf{u} = 0$). The solution to (1) would require boundary conditions for $\boldsymbol{\xi}$ on $\partial\mathcal{D}$; there is no unique expression for this to be derived from the velocity condition $\mathbf{u} = 0$ on $\partial\mathcal{D}$. On the other hand one may try to understand the vorticity

0021-9991/00 $35.00

boundary condition in terms of a physical process. A family of Lagrangian numerical methods (e.g., see [7]) has been developed in which one of the boundary conditions to be satisfied by $\mathbf{u}$ at a wall (this is namely the no-slip condition) is represented in terms of vorticity creation there. This is to give algorithmic expression to an idea which has been proposed a number of times in earlier literature (e.g., see [19, 25], or see Stokes' letter in [32, Sect. 643]). The flow which evolves from this creation principle is typically represented in terms of the kinematics of an ensemble of point vortex elements whose singularity is ameliorated by a smoothing strategy.

The robustness of vortex methods in two dimensions derives from the Hamiltonian nature of the underlying Euler flow problem. Unfortunately this Hamiltonian property does not generalize in a simple way to corresponding point vortex elements in three dimensions. The dilemma of generalizing a Lagrangian representation of a continuum vorticity field from two into three dimensions can be understood as one of finding a consistent relationship between a vorticity field which is macroscopic and extensive, and a Lagrangian "particle" of compact support. In two dimensions geometrical symmetry resolves the problem for us: vorticity extends in directions perpendicular to the plane of flow so a representation of the continuum field in terms of point vortices is consistent with the extensive character of the field. It is precisely this which is lost in a generalization to three dimensions where one expects (by virtue of the solenoidality of $\boldsymbol{\xi}$) the lines of equivorticity to extend throughout the fluid in macroscopic closed filaments. There is a particular difficulty when we come to reconcile such a global, solenoidal vorticity field to its creation at a wall in response to viscous boundary conditions—conditions which express the macroscopic effect of local, molecular processes.

These facts motivate an alternative representation of flow in terms of fluid impulse density, which is to say in terms of a vector field of compact support. This formulation of the Euler problem leads to Lagrangian representations which are Hamiltonian in three dimensions (see [5, 6]). Furthermore, problems characterized by slight viscosity can be cast as a dissipative perturbation of the Hamiltonian dynamics (see [30, 31]).

In the present note we develop, in two dimensions, a representation of viscous boundary conditions in terms of the creation of impulse at the wall. In contrast to standard vortex methods, this representation generalizes naturally into three dimensions.

The velocity wall condition $\mathbf{u} = \mathbf{0}$ may be expressed in terms of a wall impulse which is oriented parallel to the boundary, or alternatively, it may be oriented normally to the boundary. The former case we can associate with the creation of a vortex doublet sheet, the latter with the creation of a vortex (monopole) sheet. We illustrate these two cases numerically in Sections 6 and 7.

2. EQUATIONS OF MOTION

We define impulse density, $\mathbf{m}$, through the relationship

$$\mathbf{u} = \mathbf{m} + \nabla\phi, \tag{2}$$

where $\mathbf{u}$ is the divergence-free velocity field, and where we understand ϕ to be a scalar function and $\nabla\phi$, being curl-free, is an irrotational field. In the literature a variety of nomenclatures is attached to $\mathbf{m}$: "vortex momentum density" [17], "velicity" [5], "magnetization variable" [6], and "impetus variable" [20].

Implicit to Eq. (2) is the general property of Hodge decomposition [27]: any vector (**m**) can be decomposed into the sum of two vectors, one of which is divergence-free (**u**), and other curl-free ($\nabla\phi$). It is in this particular sense that we will refer to (2) as a "decomposition of **m**." The expression (2) also resembles a Helmholtz decomposition of velocity into irrotational and non-irrotational parts. It is important to note that we do not imply by this that **m** is divergence-free: although the variable **m** has the physical dimensionality of velocity, it is more usefully understood as an impulse density.

The field **m** is of compact support: it is this property which implies it is an impulse "density," since in this case it is formally related to fluid impulse, **I**, through

$$\mathbf{I} = \iiint_V \mathbf{m}\, dV$$

[5, 6, 10, 26]. Vorticity is related to **m** through $\boldsymbol{\xi} = \nabla \times \mathbf{m}$. An equation of motion can be determined [23, 5, 6, 9, 10] for **m** in the case of an incompressible viscous fluid by substituting **u** from (2) into the non-dimensionalized Navier–Stokes equation. Upon substitution we find

$$\frac{D\mathbf{m}}{Dt} + (\nabla\mathbf{u})^T\mathbf{m} - \frac{1}{Re}\Delta\mathbf{m} = \nabla\left(\frac{D\phi}{Dt} + \frac{1}{2}\mathbf{u}\cdot\mathbf{u} - p - \frac{1}{Re}\Delta\phi\right) = \nabla\Lambda$$

(where the ij element of the matrix $(\nabla\mathbf{u})^T$ is $\partial u_j/\partial x_i$ and p is pressure). Upon choice of gauge $\Lambda = 0$ we determine two consistent equations. We determine

$$\frac{D\mathbf{m}}{Dt} = -(\nabla\mathbf{u})^T\mathbf{m} + \frac{1}{Re}\Delta\mathbf{m} \tag{3}$$

and note that this equation of motion does not involve ϕ.

We also determine the equation

$$\frac{D\phi}{Dt} = -\frac{1}{2}|\mathbf{u}|^2 + p + \frac{1}{Re}\Delta\phi, \tag{4}$$

which is a transport equation for ϕ in which pressure, p, appears explicitly; the variable **m** does not appear however. This separation of the Navier–Stokes equation into Eqs. (3) and (4) is obviously not unique, but follows upon the particular choice of gauge, $\Lambda = 0$. Smereka and Russo [26] describe this choice as the "geometric gauge." It is the most widely studied case (e.g., [5, 6, 10]), and its geometric properties suggest it is the most appropriate gauge for Lagrangian models of flow. (In the case of Euler flow, the oriented surface to be associated with **m** is "frozen into" the fluid [26].) In any case, choice of gauge should not affect the velocity solution to the Navier–Stokes problem.

Since we are interested in incompressible flow, and in applying boundary conditions at fixed instants of time, we can apply the divergence operator to (2) and, if we note $\nabla\cdot\mathbf{u} = 0$, we determine a more useful equation for our purpose: given, at an instant of time t_o, a known distribution of impulse in the flow denoted by **m**, the function ϕ will satisfy the Poisson equation

$$\Delta\phi = -\nabla\cdot\mathbf{m}. \tag{5}$$

This Poisson problem is well posed if appropriate boundary conditions are specified for ϕ. If a gradient condition is prescribed, ϕ is determinable only to an additive constant;

however, we will use the fact that the field $\nabla\phi$—and hence the decomposition (2)—is uniquely determined in such a case.

3. TWO DECOMPOSITIONS AT THE BOUNDARY

3.1. Viscous boundary conditions at a solid wall. At a solid wall $\partial\mathcal{D}$ with unit normal $\mathbf{n}$ and unit tangential vector $\mathbf{s}$, the wall conditions $\mathbf{u}\cdot\mathbf{n}=0$ (impermeability) and $\mathbf{u}\cdot\mathbf{s}=\mathbf{0}$ (no-slip) imply from (2) the union of conditions

$$\left.\begin{aligned}\mathbf{m}\cdot\mathbf{n} &= -\partial\phi/\partial n\\ \mathbf{m}\times\mathbf{n} &= -\partial\phi/\partial s\ \mathbf{s}\end{aligned}\right\} \quad \text{on } \partial\mathcal{D}. \tag{6}$$

Thus if we are to solve (3) we will need to specify the gradients of ϕ at $\partial\mathcal{D}$. Two obvious simplifications result if we choose, in turn, each of the gradients in (6) to vanish, i.e., if we choose ϕ so that on $\partial\mathcal{D}$

$$\left.\begin{aligned}\mathbf{m}\cdot\mathbf{n} &= 0\\ \mathbf{m}\times\mathbf{n} &= -\partial\phi/\partial s\ \mathbf{s}\end{aligned}\right\} \tag{7}$$

or alternatively

$$\left.\begin{aligned}\mathbf{m}\cdot\mathbf{n} &= -\partial\phi/\partial n\\ \mathbf{m}\times\mathbf{n} &= 0\end{aligned}\right\}. \tag{8}$$

We note that the choice $\partial\phi/\partial s = 0$ invoked in (8) implies, upon surface integration over the boundary, a Dirichlet condition for ϕ. On the other hand, $\partial\phi/\partial n = 0$ in (7) is a Neumann condition. These two gradient conditions each determine a unique Hodge decomposition of $\mathbf{m}$ at the wall. Conditions (7) imply an impulse density $\mathbf{m}$ which is tangential at the wall; conditions (8) imply an impulse density oriented normally at the wall. We denote the wall impulse density associated with conditions (7) as $\mathbf{m}_I$ and that with (8) as $\mathbf{m}_{II}$; furthermore we associate these with scalar functions ϕ_I, and ϕ_{II}, respectively.

On the basis of the foregoing discussion, we can now construct two decompositions. Given a distribution of impulse in the flow, $\mathbf{m}$, we can, from Eq. (5), determine a function ϕ_I satisfying the Poisson equation

$$\Delta\phi_I = -\nabla\cdot\mathbf{m} \tag{9}$$

together with the boundary condition $\partial\phi_I/\partial n = 0$ on $\partial\mathcal{D}$. From this function ϕ_I we can determine an irrotational velocity field $\mathbf{u}_I$ such that

$$\mathbf{u}_I = \nabla\phi_I$$

which, by virtue of our particular choice of ϕ satisfies the following conditions at the wall:

$$\mathbf{u}_I\cdot\mathbf{n} = 0 \tag{10}$$

$$\mathbf{u}_I\cdot\mathbf{s} = -\mathbf{m}_I\cdot\mathbf{s}. \tag{11}$$

Similarly for the ϕ_{II} case we deduce from (5)

$$\Delta\phi_{II} = -\nabla \cdot \mathbf{m}$$

together with the boundary condition $\partial\phi_{II}/\partial s = 0$ on $\partial\mathcal{D}$. In this case we determine an irrotational field $\mathbf{u}_{II} = \nabla\phi_{II}$ satisfying at the wall

$$\mathbf{u}_{II} \cdot \mathbf{n} = -\mathbf{m}_{II} \cdot \mathbf{n} \tag{12}$$

$$\mathbf{u}_{II} \cdot \mathbf{s} = 0. \tag{13}$$

At a fixed time and for a given distribution $\mathbf{m}$ in the flow, we can thus solve two well-posed Poisson equations for ϕ_I and ϕ_{II} and hence determine two irrotational fields $\mathbf{u}_I$ and $\mathbf{u}_{II}$ which at the wall are parallel to, and normal to $\partial\mathcal{D}$, respectively. These irrotational fields, by construction, satisfy one of the two boundary conditions—impermeability (10) or no-slip (13).

It remains to give meaning to the complementary boundary conditions (11) and (12). These two conditions imply the existence of wall impulse vectors $\mathbf{m}_I$ and $\mathbf{m}_{II}$, respectively. In each case, having solved for irrotational fields $\mathbf{u}_I$ and $\mathbf{u}_{II}$, we are in a position to deduce—from (11) and (12)—the magnitude and orientation of $\mathbf{m}_I$ and $\mathbf{m}_{II}$. This constitutes a strategy for relating the viscous boundary condition $\mathbf{u} = \mathbf{0}$ to the imparting of impulse to the flow.

3.2. Heuristic interpretation of $\mathbf{m}_I$ *and* $\mathbf{m}_{II}$. Although $\mathbf{m}_I \cdot \mathbf{s}$ on $\partial\mathcal{D}$ can be determined from the boundary conditions as we have described, no knowledge of $\mathbf{m}_I$ away from $\partial\mathcal{D}$ can be derived from these conditions. This implies we cannot construct the normal gradient of $\mathbf{m}_I$ exclusively from the boundary conditions, nor can we construct a wall vorticity. (For example, if $\mathbf{m}_I$ is strictly tangential to a planar boundary $\partial\mathcal{D}$, we define wall vorticity there as

$$\boldsymbol{\xi} = \nabla \times m_I\mathbf{s} = -\partial m_I/\partial n\ \mathbf{k}$$

with $\mathbf{k} = \mathbf{n} \times \mathbf{s}$; but, as we explain, such a normal derivative cannot be inferred from the boundary condition.) The condition $\mathbf{u}_I \cdot \mathbf{s} = -\mathbf{m}_I \cdot \mathbf{s} \neq 0$ implies a sheet discontinuity in tangential impulse at $\partial\mathcal{D}$, which we express as a horizontal "impulse sheet" of magnitude m_I. For example, in the case where there is no initial impulse in the flow ($\mathbf{m} = \mathbf{0}$, and ϕ_I is harmonic) the implication of $\mathbf{u}_I \cdot \mathbf{s} = -\mathbf{m}_I \cdot \mathbf{s}$ is that, confined to the surface $\partial\mathcal{D}$, there is non-zero tangential impulse with the obvious implication that this must be a thin doublet sheet.

The $\mathbf{m}_{II}$ case invites a contrasting interpretation. The impulse density $\mathbf{m}_{II}$ serves as a vector potential for tangential vorticity at the wall. Again, to take the case of a plane surface we define

$$\boldsymbol{\xi} = \nabla \times m_{II}\mathbf{n} = \partial m_{II}/\partial s\ \mathbf{k} \qquad \text{on } \partial\mathcal{D}.$$

Such a lateral derivative can be inferred from the boundary condition. Thus the creation of a thin sheet of normal impulse at the wall is equivalently a sheet of wall vorticity. In the two-dimensional context, we can understand this sheet of normally oriented impulse in terms of a system of vortex pairs whose pair-axes are aligned parallel to the wall. This is equivalent to a system of coplanar vortex monopoles.

The decompositions proposed in Subsection 3.1 reflect two natural symmetries in the boundary value problem. We infer from the present discussion that a solid wall in contact with a viscous flow is a generating surface for impulse dipoles. We have described two modes of generation, both of which are consistent with the wall condition $\mathbf{u} = \mathbf{0}$. We also note that these can be superposed.

Taken in a Lagrangian sense, the consequences (to the evolution of interior flow) of this superposition at the wall can be modeled by an ensemble of $\mathbf{m}_I$ and $\mathbf{m}_{II}$ objects interacting with each other (i.e., moving in each other's induced velocity fields). The dimensional implications of each decomposition (see Section 4) imply that this will reflect, at least in part, an interaction between different scales in the flow. The notion that fluid flow can be numerically modeled by a superposition of fields induced by vortex sheets and vortex-dipole sheets was introduced (in the unbounded, inviscid setting of free shear layers) by Krasny [16].

4. CONSIDERATIONS OF DIMENSIONAL SCALE

4.1. Bounded flow in two dimensions. In the $x - y$ plane we consider a wall at $y = 0$ with $y > 0$ occupied by fluid; $\mathbf{i}$ and $\mathbf{j}$ represent unit vectors in the x and y directions, respectively. By way of approximation, we shall conceive of a regime in the neighborhood of the wall in which the impulse field $\mathbf{m}$ is constrained according to (7)—i.e., the $\mathbf{m}_I$ case; or, alternatively, to (8)—i.e., the $\mathbf{m}_{II}$ case.

We could conceive of an array of vortex pairs and, consistent with a presumed thinness of this doublet sheet, it can be subjected to the limiting procedure

$$\mathcal{M}(x) = \lim_{\substack{d \to 0 \\ \Gamma \to \infty}} \Gamma d, \tag{14}$$

where the bounded limit $\mathcal{M}(x)$ represents the tangential impulse per unit length of wall and Γ is the modulus of the circulation of each vortex in the pair; d is the dipole separation. By way of determining the sign of vorticity, the pairs will be created in such a way that impulse is oriented in the direction $-\mathbf{u}_I(x, 0) \cdot \mathbf{s}$. Figure 1 illustrates schematically the situation for the case of uniform flow over a wall (the filled circles represent vortices of negative sign).

The $\mathbf{m}_{II}$ case follows in a similar manner: consistent with $\mathbf{m} \times \mathbf{n} = \mathbf{0}$. We identify a normal component of wall impulse to be $m_y(x, 0) = -\mathbf{u}_{II} \cdot \mathbf{n}$, from which we can construct a wall vorticity $\xi(x, 0) = \partial m_y / \partial x$ on $\partial \mathcal{D}$.

The equivalence of this to a system of monopoles is illustrated in Fig. 2 and is formally established by taking a center difference of m_y with respect to x. Except in the case of a closed boundary, the endpoints are excluded from this differencing.

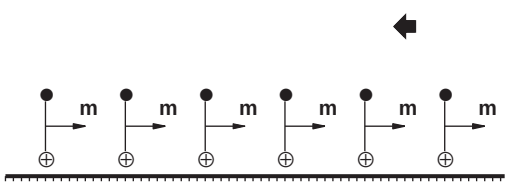

FIG. 1. Schematic distribution of vortex dipoles created over a surface in response to a uniform slip velocity flowing from right to left.

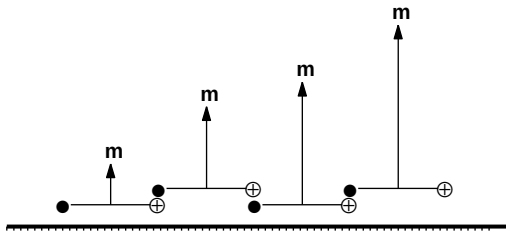

FIG. 2. Schematic distribution of vortex pairs in the case of $\mathbf{m}_{II}$, impulse density increasing linearly as x. This is equivalent to an array of monopoles of uniform orientation and strength.

Having constructed $\xi(x, 0)$ from $m_y(x, 0)$, we can conceive of this wall vorticity as a created thin vortex sheet with strength (or linear circulation density) $\kappa(x)$ such that

$$\kappa(x) = \lim_{d\to 0} \int_0^d \frac{\partial}{\partial y} u_x(x, y)\, dy. \tag{15}$$

The creation procedure we introduce here for $\mathbf{m}_{II}$, in itself, conserves global circulation since vortex *pairs* are created. Once wall vorticity is created it is then subject to viscous transport across the streamline $\partial\mathcal{D}$; it is *this* mechanism which evolves the circulation of the flow. It is important to note that this change in circulation proceeds on a local, diffusive scale (see the discussion in Subsection 5.2 of Batchelor [2]) and is not to be governed by a non-local, elliptic operator such as that associated with a Poisson equation. (The three-dimensional analogue of a "vortex pair" is a "vortex loop": the implication of representing the viscous boundary condition in terms of the creation of vortex loops is that, in three dimensions, the created vorticity is naturally solenoidal.)

4.2. Dimensional scale for $\mathbf{m}_{II}$. Consistent with our present discussion, we consider a near-wall fluid regime of thickness δ over a boundary at $y = 0$. The scale of the lateral variable is $x \sim O(1)$; the normal length scale is $y \sim O(\delta)$. These dimensional considerations imply the following: $\partial u_x/\partial t \sim O(1)$; $u_x \sim O(1)$; $\partial u_x/\partial x \sim O(1)$. The continuity condition $\nabla \cdot \mathbf{u} = 0$ implies then that $\partial u_y/\partial y \sim O(1)$, hence $u_y \sim O(\delta)$. Furthermore, $\partial p/\partial x \sim O(1)$ and $\partial p/\partial y \sim O(\delta)$. We can apply these dimensional considerations to the non-dimensional Navier–Stokes equation, in Cartesian component form, to determine the Prandtl boundary layer equations.

From this we can infer the dimensional scale of vorticity by observing that

$$\xi = \frac{\partial u_x}{\partial y} - \frac{\partial u_y}{\partial x}$$

and deducing that $\xi \sim \max(O(\frac{1}{\delta}), O(\delta)) = O(\frac{1}{\delta})$. This applied to the non-dimensional vorticity transport equation leads to the vorticity analogue of the Prandtl equation (see [7]), namely

$$\frac{D\xi}{Dt} = \frac{1}{Re} \frac{\partial^2 \xi}{\partial y^2}. \tag{16}$$

By the same token we can infer the dimensional scale of impulse density, **m**. From the fact that $\nabla \times \mathbf{m} = \boldsymbol{\xi}$, we infer

$$\frac{\partial m_x}{\partial y} - \frac{\partial m_y}{\partial x} \sim O\left(\frac{1}{\delta}\right).$$

Choosing the maximal dimensions for each term to determine dimensional consistency, we determine $m_x \sim O(1)$; $m_y \sim O(\frac{1}{\delta})$.

4.3. Dimensional scale for $\mathbf{m}_I$. We propose now a complementary dimensional model to that of Prandtl. In this setting $x \sim O(\epsilon)$, $y \sim O(1)$, $\partial u_x/\partial t \sim O(\epsilon)$; $\partial u_x/\partial x \sim O(1)$; $\partial u_y/\partial y \sim O(1)$, hence $u_y \sim O(1)$. Furthermore, $\partial p/\partial x \sim O(\epsilon)$ and $\partial p/\partial y \sim O(1)$. Applied to the Navier–Stokes equation, an approximate evolution equation in primitive variables (specifically in u_y) is determined. Similarly, the dimensional scale of vorticity can be deduced from

$$\xi = \frac{\partial u_y}{\partial x} - \frac{\partial u_x}{\partial y} \sim \max\left(O\left(\frac{1}{\epsilon}\right), O(\epsilon)\right).$$

The corresponding dimensional scale of impulse density is inferred (as before in subsection 3.1) from its relationship to vorticity; in this case we have

$$\frac{\partial m_y}{\partial x} - \frac{\partial m_x}{\partial y} \sim O\left(\frac{1}{\epsilon}\right).$$

Thus, following the same policy as before we deduce $m_x \sim O(\frac{1}{\epsilon})$ and $m_y \sim O(1)$.

5. LAGRANGIAN REPRESENTATION

5.1. Thin sheet elements: The $\mathbf{m}_{II}$ *case.* At any given time-step we postulate the existence at the wall of a vortex sheet such that the wall vorticity is $\xi = \partial m_y/\partial x$. To achieve an ensemble of Lagrangian elements of compact support the sheet is partitioned into elements each of length l and centered at points (x_o, y_o). Consistent with a mid-point rule approximation of interior elements, we can consider each sheet element to have a constant vortex sheet strength κ. An approximation to the velocity field induced by such an element was introduced by Chorin in [8], but in order to provide a unified treatment we pursue here an alternative approach to approximating the velocity field of a vortex sheet, similar to that employed by [15] and others. This is to specialize the Biot–Savart integral to the case of a horizontal plane sheet element of uniform strength, κ, and length l centered at (x_o, y_o); we have

$$\mathbf{u}(x, y) = \frac{\kappa}{2\pi} \int_{-l/2}^{l/2} \frac{(y_o - y, -(x' + x_o - x))}{|\mathbf{r}'|^2}\, dx' \tag{17}$$

with $|\mathbf{r}'| = (x' + x_o - x)\mathbf{i} + (y_o - y)\mathbf{j}$. The components of velocity, $\mathbf{u} = (u_x, u_y)$, can be determined explicitly as

$$u_x(x, y) = \frac{\kappa}{2\pi}\left\{\tan^{-1}\left(\frac{x_o - x + l/2}{y_o - y}\right) - \tan^{-1}\left(\frac{x_o - x - l/2}{y_o - y}\right)\right\} \tag{18}$$

$$u_y(x, y) = \frac{\kappa}{2\pi}\log\left\{\frac{(x_o - x - l/2)^2 + (y_o - y)^2}{(x_o - x + l/2)^2 + (y_o - y)^2}\right\}^{\frac{1}{2}}. \tag{19}$$

The tangential component is proportional to the angle subtended at (x, y) by a horizontal sheet of length l centered at (x_o, y_o).

To confirm that such a monopole sheet element is related to an impulse vector oriented normally to the sheet, we can specialize the definition of impulse, **I**, to the case of a thin horizontal vortex sheet of length l centered at (x_o, y_o). In two dimensions impulse is defined (see, for example, article 152 of [18]) as

$$\mathbf{I} = \int\int_A \mathbf{r} \times \boldsymbol{\xi}\, dA,$$

where we take A to be an area adjacent to the wall containing the vortex sheet element. This element is of compact support and occupies the line $x \in (-l/2, l/2)$ on $y = 0$. We take wall vorticity to be $\boldsymbol{\xi} = -\partial u_x/\partial y\, \mathbf{k}$ there. If we consider this area to be a rectangle of width l and height d (i.e., an "overburden" of area ld above the wall) we can determine the impulse associated with this area as

$$\mathbf{I} = \int_0^d \int_{-l/2}^{l/2} \left\{ -(y - y_o)\frac{\partial u_x}{\partial y}\mathbf{i} + (x - x_o)\frac{\partial u_x}{\partial y}\mathbf{j} \right\} dx\, dy.$$

We reverse the order of integration and take into account the thin-sheet support of $\boldsymbol{\xi}$ by taking the limit $d \to 0$ so that

$$\mathbf{I} = -\mathbf{i} \int_{-l/2}^{l/2} \left\{ \lim_{d\to 0} \int_0^d (y - y_o)\frac{\partial u_x}{\partial y}\, dy \right\} dx + \mathbf{j} \int_{-l/2}^{l/2} (x - x_o) \left\{ \lim_{d\to 0} \int_0^d \frac{\partial u_x}{\partial y}\, dy \right\} dx.$$

The inner integral of the **i**-component can be integrated by parts and, if we require u_x at the wall to be bounded—consistent with (18)—this integral vanishes in the limit. Invoking the definition of a vortex sheet (15), we have simply

$$\mathbf{I} = \kappa \mathbf{j} \int_{-l/2}^{l/2} (x - x_o)\, dx = -x_o l \kappa \mathbf{j},$$

where κ is the sheet strength (circulation per unit length of the sheet). This is the impulse we associate with area A; we divide by this area to obtain an impulse density:

$$\mathbf{m} = m_y \mathbf{j} = -\frac{x_o \kappa}{d}\mathbf{j}. \tag{20}$$

Thus the impulse density to be associated with a tangentially oriented vortex sheet embedded in an area of fluid, A, is itself oriented normal to the sheet, as we would expect from dimensional considerations. Differentiating m_y from (20) with respect to x_0 we recover the vorticity of the sheet $\xi = -\kappa/d$.

5.2. Thin sheet elements: The $\mathbf{m}_I$ *case.* Following the discussion of subsection 4.1 we introduce a thin dipole sheet which can be visualized as a doublet consisting of a vortex sheet (S_1) of uniform strength κ separated by a uniform distance d from a vortex sheet (S_2) of strength $-\kappa$. To determine the velocity field induced by an element of a partitioned thin dipole sheet, we propose to evaluate the field due to the doublet, then take a limit $d \to 0$ as described by Eq. (14).

We denote points on S_1 as $\mathbf{x}' = (x', y')$; hence points on S_2 are expressed as $\mathbf{x}'' = \mathbf{x}' - \mathbf{n}d$, where $\mathbf{n}$ is the unit normal to the double sheet at $\mathbf{x}'$. The stream function at $\mathbf{x} = (x, y)$ for this double sheet is

$$\psi(\mathbf{x}) = -\frac{\kappa}{2\pi} \int_{S_1} \{\ln|\mathbf{x}' - \mathbf{x}| - \ln|\mathbf{x}' - \mathbf{x} - \mathbf{n}d|\}\, d\mathbf{x}'.$$

Toward representing such a sheet by a sum of Lagrangian elements of compact support we pursue a similar partitioning strategy to that introduced in the previous section. For the horizontal component of velocity at position $\mathbf{x} = (x, y)$ induced by a flat sheet aligned in the x-direction, we have

$$u_x(x, y) = \frac{\partial \psi}{\partial y} = \frac{\kappa}{2\pi} \int_{S_1} \left\{ \frac{y' - y}{|\mathbf{x}' - \mathbf{x}|^2} - \frac{y' - y - d}{|\mathbf{x}' - \mathbf{x} - \mathbf{n}d|^2} \right\} d\mathbf{x}'.$$

Upon partition we consider a sheet element of length l centered at $\mathbf{x}' = (0, y_o)$, so that

$$u_x(x, y) = \frac{\kappa}{2\pi}(y_o - y) \int_{-l/2}^{l/2} \left\{ \frac{1}{|\mathbf{x}' - \mathbf{x}|^2} - \frac{1}{|\mathbf{x}' - \mathbf{x} - \mathbf{n}d|^2} \right\} dx' + \frac{\kappa d}{2\pi} \int_{-l/2}^{l/2} \frac{1}{|\mathbf{x}' - \mathbf{x} - \mathbf{n}d|^2}\, dx'. \tag{21}$$

Jackson [13, p. 36] notes how integrals such as these may be approximated for small d. For $|\mathbf{x}| \gg |\mathbf{a}|$ we have

$$\frac{1}{|\mathbf{x} + \mathbf{a}|^2} \simeq \frac{1}{|\mathbf{x}|^2} \left\{ 1 - \frac{2\mathbf{a} \cdot \mathbf{x}}{|\mathbf{x}|^2} + \cdots \right\}.$$

Applying this in the present context, the first integral of (21) becomes

$$-\frac{\kappa}{2\pi}(y_o - y) \int_{-l/2}^{l/2} \frac{1}{|\mathbf{x}' - \mathbf{x}|^2} \left\{ \frac{2d\mathbf{n} \cdot (\mathbf{x}' - \mathbf{x})}{|\mathbf{x}' - \mathbf{x}|^2} \right\} dx',$$

while the second becomes

$$\frac{\kappa d}{2\pi}(y_o - y) \int_{-l/2}^{l/2} \frac{1}{|\mathbf{x}' - \mathbf{x}|} \left\{ 1 + \frac{2d\mathbf{n} \cdot (\mathbf{x}' - \mathbf{x})}{|\mathbf{x}' - \mathbf{x}|^2} \right\} dx'.$$

Neglecting terms of $O(d^2)$ we write (21) as

$$u_x(x, y) = -\frac{\kappa d}{\pi}(y_o - y) \int_{-l/2}^{l/2} \frac{\mathbf{n} \cdot \hat{\mathbf{x}}}{|\mathbf{x}' - \mathbf{x}|^3}\, dx' + \frac{\kappa d}{2\pi} \int_{-l/2}^{l/2} \frac{1}{|\mathbf{x}' - \mathbf{x}|^2}\, dx',$$

where $\hat{\mathbf{x}}$ is the unit vector in the direction $\mathbf{x}' - \mathbf{x}$. We can understand the numerator of the first integrand geometrically since $-\mathbf{n} \cdot \hat{\mathbf{x}}$ is the cosine of the angle θ indicated in Fig. 3.

We follow [13] and formally take the limit of vanishing thickness

$$\lim_{\substack{d \to 0 \\ \kappa \to \infty}} \kappa d = \mathcal{M},$$

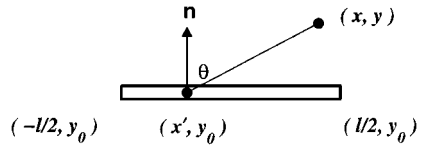

FIG. 3. Geometry of dipole sheet element centered at $(0, y_o)$.

where the bounded limit $\mathcal{M}$ represents here a tangential "impulse per unit length" associated with the dipole sheet. We can proceed to perform the integration by making a substitution of variables $x' - x = (y_o - y)\tan\theta$ where θ is the angle indicated in Fig. 3 to determine

$$u_x(x,y) = \frac{\mathcal{M}}{\pi(y_o - y)}\left\{\tan^{-1}\left[\frac{l/2 - x}{y_o - y}\right] - \tan^{-1}\left[\frac{-l/2 - x}{y_o - y}\right]\right\}$$
$$+ \frac{\mathcal{M}}{2\pi}\left\{\frac{l/2 - x}{(l/2 - x)^2 + (y_o - y)^2} - \frac{-l/2 - x}{(-l/2 - x)^2 + (y_o - y)^2}\right\}. \quad (22)$$

The formula for a sheet centered at (x_o, y_o) follows by substituting $x - x_o$ for x in (22).

The vertical component of velocity is to be determined in a similar fashion from

$$u_y(x,y) = -\frac{\partial\psi}{\partial x} = -\frac{\kappa}{2\pi}\int_{-l/2}^{l/2}(x' - x)\left\{\frac{1}{|\mathbf{x}' - \mathbf{x}|^2} - \frac{1}{|\mathbf{x}' - \mathbf{x} - \mathbf{n}d|^2}\right\}dx'$$
$$= -\frac{\kappa d}{\pi}\int_{-l/2}^{l/2}\frac{(x' - x)\mathbf{n}\cdot\hat{\mathbf{x}}}{|\mathbf{x}' - \mathbf{x}|^3}\,dx'.$$

Taking the thin sheet limit and equating $\mathbf{n}\cdot\hat{\mathbf{x}} = (y_o - y)/|\mathbf{x}' - \mathbf{x}|$, we get

$$u_y(x,y) = -\frac{\mathcal{M}(y_o - y)}{\pi}\int_{-l/2}^{l/2}\frac{(x' - x)}{\left[(x' - x)^2 + (y_o - y)^2\right]^2}\,dx'$$
$$= \frac{\mathcal{M}(y_o - y)}{2\pi}\left\{\frac{1}{(l/2 - x)^2 + (y_o - y)^2} - \frac{1}{(-l/2 - x)^2 + (y_o - y)^2}\right\}. \quad (23)$$

It is proposed to represent the solution of (3) in terms of elements of tangential impulse density derived from partitioning a dipole sheet. We ascribe to this sheet an impulse per unit length of $\mathcal{M} = -\mathbf{u}_I \cdot \mathbf{s}l$ with $\mathbf{u}_I \cdot \mathbf{s}$ evaluated at the mid-point of the sheet of length l. An ensemble of such elements interacts according to Eqs. (22) and (23).

5.3. Singularity. We have explicitly performed the Biot–Savart integration expressed in Subsections 5.1 and 5.2. We note that whereas the strength of $\mathbf{m}_I$ and $\mathbf{m}_{II}$ sheets are related to fields $\mathbf{u}_I$ and $\mathbf{u}_{II}$, respectively, the velocity field *induced* by these sheet objects is not in any sense "equal" to $\mathbf{u}_I$ or $\mathbf{u}_{II}$. Rather, the induced fields have, in each case, a spatial structure with source-point singularity.

In the case of $\mathbf{m}_{II}$, from (18) the induced field component u_x satisfies a condition of regularity; u_y on the other hand, from (19), admits logarithmic singularity at the end-points $(x_o \pm l/2, y_o)$. This is most directly smoothed (see [15]) by introducing an additive smoothing parameter, δ_{II}, into the denominator of the integrand of (17). This approach will serve our present purpose, although a more rigorous treatment of smoothing is available

for this $\mathbf{m}_{II}$ case (see [4]), which is achieved by convolving the integrand of (17) with a smoothing kernel [3]. The logarithmic edge singularity of (19) is a result of the partitioning of the vortex sheet (an equivalent smooth contiguous sheet does not admit this singularity). This situation may be distinguished in character from the singularities arising in standard blob methods in which the singular integrand of (17) is ameliorated, and hence made the subject of a numerical quadrature.

The doublet-sheet $\mathbf{m}_I$-elements we have introduced in subsection 5.2 also admit singularity in the fields they induce. Specifically, the function $\psi(\mathbf{x})$ is discontinuous across the sheet; therefore the normal derivative $\partial\psi/\partial y$ (and hence u_x) is singular on the sheet itself. The normal velocity component u_y is singular at the points $(x_o \pm l/2, y_o)$.

The induced field in the case of $\mathbf{m}_I$ elements does not consist of a point singularity, but rather a singularity on $y = y_o$, for $|x - x_o| \leq l/2$. Were we to convolve the relevant Biot–Savart kernel with a smoothing function, we could reasonably require this function to contract, upon refinement, to a line rather than to a point. As in the $\mathbf{m}_{II}$ case we shall take the alternative approach of incorporating a smoothing parameter into the integrand of the Biot–Savart integral.

5.4. Integration in time. As time progresses, thin vortex and/or vortex-dipole sheets are created at the beginning of each time step (the discretized increment of time is dt) on a solid boundary consistent with viscous boundary conditions. In either case the sheets are each partitioned into sheet-elements of uniform length l_I and l_{II}, respectively. From the dimensional considerations of Section 4, we expect typically $l_I \ll l_{II}$.

After creation, these sheet elements diffuse from the wall over time step dt into the flow interior; this viscous diffusion process is modeled here by imparting to each element a random walk displacement (of zero mean, and variance $2dt/Re$) as it evolves. In subsequent time-steps, the elements are also translated in the velocity field induced by the particle ensemble. Consider a planar wall at $y = y_o$. In the case of vortex sheets the relevant velocity field is determined by (18) and (19); in the case of vortex-dipole sheets, by (22) and (23). Adopting the approach to smoothing described in [15] (and specifying relevant smoothing parameters, e.g., $\delta_{II} \sim l_{II}/2$) we express the horizontal velocity field induced at a point $\mathbf{x} = (x, y)$ due to an ensemble of N vortex sheet elements of strength $\{\kappa_j\}$ centered, at time t, at positions $\mathbf{x}_j(t) = (x_j(t), y_j(t))$,

$$\mathbf{u}(\mathbf{x}, t) = \sum_{j=1}^{N} \kappa_j \mathbf{K}(\mathbf{x} - \mathbf{x}_j(t)).$$

The integrated Biot–Savart kernels $\mathbf{K} = (K_x, K_y)$ for the case of vortex sheets are deduced from (18) and (19). Applied to each sheet in the ensemble, this leads to an evolving N-body Lagrangian system of elements. The trajectory of the ith element is approximated from a numerical solution to the system of ordinary differential equations

$$\begin{aligned} \frac{d\tilde{\mathbf{x}}_i(t)}{dt} &= \sum_{j=1}^{N} \kappa_j \mathbf{K}(\tilde{\mathbf{x}}_i(t) - \tilde{\mathbf{x}}_j(t)) \\ \tilde{\mathbf{x}}_i(0) &= \alpha_i, \end{aligned} \tag{24}$$

where, at time t, the location $\tilde{\mathbf{x}}_i = (\tilde{\mathbf{x}}_i(t), \tilde{y}_i(t))$ is determined by solving the system (24)

using, for example, Runge–Kutta integration. The initial location of the element is the wall itself, i.e., $\alpha_i = (x_o, y_o)$ for some $x_o \in [0, L]$, and $y_o = 0$.

A similar system (in terms of integrated kernels $\mathbf{L}$) can be developed for the case of an ensemble of $\boldsymbol{M}$ vortex-dipole sheets (see Subsection 6.2).

As time progresses, the strength of an impulse sheet in the flow interior must evolve according to (3). The evolution of local Cartesian components (m_x, m_y) associated with a particular element can be interpreted as an evolution in its strength $(\mathcal{M})$ and a rotation about its centroid. We express system (3) for vortex dipole sheets by the following "splitting": Euler advection is modeled as

$$\frac{D}{Dt}\mathbf{m}_I = 0,$$

and viscous diffusion,

$$\frac{\partial}{\partial t}\mathbf{m}_I = \frac{1}{Re}\Delta\mathbf{m}_I.$$

To these are added the evolution of impulse strength implied by

$$\frac{\partial}{\partial t}\mathbf{m}_I = -(\nabla\mathbf{u})^T\mathbf{m}_I, \tag{25}$$

where this latter splitting bears analogy to a common treatment of vorticity stretching in three dimensions (discussed, for example, in [12]).

We will illustrate the $\mathbf{m}_{II}$ decomposition by modeling flow past a circular cylinder. This requires treatment of flow far from the wall, such as that flow associated with the wake. We expect vortex sheet elements to rotate in the stream of such interior flow. The interaction equations must be adapted accordingly. We attach to each sheet a direction cosine pair, e.g., $(\cos\theta_i, \sin\theta_i)$ where θ_i is the angle the ith sheet-normal makes with the x-axis.

We hence adapt Eq. (24) to represent the field induced by an ensemble of generally oriented vortex sheets of strengths $\{\kappa_j\}$ so that

$$\mathbf{u}(\mathbf{x}, t) = \sum_{j=1}^{M} \kappa_j \mathsf{R}_j \mathbf{K}\left(\mathsf{R}_j^{-1}(\mathbf{x} - \mathbf{x}_j(t))\right)$$

with rotation operator given by

$$\mathsf{R}_i = \begin{pmatrix} \sin\theta_i & \cos\theta_i \\ -\cos\theta_i & \sin\theta_i \end{pmatrix}. \tag{26}$$

6. BOUNDARY LAYER FLOW—CASE OF $\mathbf{m}_I$

6.1. The limit of Blasius flow. We investigate numerically the case of boundary layer flow over a flat semi-infinite plate to illustrate the $\mathbf{m}_I$ decomposition. We could expect a single element to induce a lateral component of velocity proportional to l_I (from the angle subtended by the sheet) divided by a vertical displacement. If we take this displacement to be comparable to a viscous displacement we infer $l_I\,dt \sim O(2\,dt/Re)$.

From this we deduce

$$l_I \sim O\left(\frac{1}{Re}\right). \tag{27}$$

Our approach will be to specify a partition of the wall consistent with (27).

6.2. The field $\mathbf{u}_I$. In the present case of flow in a half-space bounded by a flat plate, we do not require to determine explicitly the solution for the function ϕ_I discussed in Subsection 3.1. For flow induced by an ensemble of M vortex sheet elements $\{\mathcal{M}_j\}$ located at points (x_j, y_j) we write the discretized Biot–Savart law as

$$\mathbf{u}(\mathbf{x}) = \sum_j^M \mathcal{M}_j \mathbf{L}(\mathbf{x} - \mathbf{x}_j(t)).$$

We can effect the condition $\mathbf{u}_I \cdot \mathbf{n} = 0$ on $\partial\mathcal{D}$ by introducing an ensemble of images $\{\mathcal{M}'_j\}$ at the reflection points $(x_j, -y_j)$ with $\mathcal{M}'_j = +\mathcal{M}_j$. The required field is thus written explicitly as

$$\mathbf{u}_I(\mathbf{x}, t) = \sum_{j=1}^M \mathcal{M}_j \mathbf{L}(\mathbf{x} - \mathbf{x}_j(t)) + \mathcal{M}_j \mathbf{L}(\mathbf{x} - \mathbf{x}'_j(t))$$

with $\mathbf{x}'_j(t) = (x_j(t), -y_j(t))$ and $\mathbf{x} \in \partial\mathcal{D}$.

6.3. Numerical results. We consider the case of uniform incident flow $U = 1$ (started impulsively at $t = 0$) over a semi-infinite flat plate occupying $y = 0$, $x > 0$. For a Reynolds number of $Re = 200$ we would expect $l_I \sim 0.005$. By way of making an initial illustration of the computational domain, we choose $l_I = 0.005$ with smoothing factor chosen to be $\delta_I = l_I/2$ and $dt = 0.1$. Figure 4 shows the distribution and size of $\mathbf{m}_I$ elements in the neighborhood of the leading edge after 50 steps have elapsed. One can see the development of a boundary layer profile. To demonstrate that this developing regime tends, upon averaging over time, to a self-similar Blasius profile, we choose four measurement locations along the plate: $x_1 = 0.25$ ($\circ$); $x_2 = 0.5$ ($\bullet$); $x_3 = 0.75$ ($\times$); and $x_4 = 1.00$ ($+$). This averaging of velocity at lateral points is intended to reveal the degree of "self-similarity," or otherwise, in the computed velocity profiles (see [8, p. 129]; or [29, 4] for similar comparisons using standard vortex sheet methods). In Fig. 5 we plot the profile of averaged velocity at each lateral location as a function of boundary layer similarity variable $\eta = y\sqrt{Re/x_m}$. At each time-step these profiles are evaluated after the created sheets have been advected and diffused. The flow

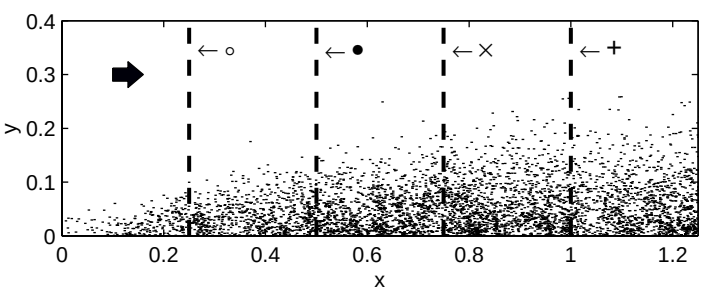

FIG. 4. Distribution of vortex dipole sheets from leading edge of a flat semi-infinite plate after 50 time-steps have elapsed ($l_I = 0.005$, $dt = 0.1$, $Re = 200$). Vertical dashed lines indicate x-locations of velocity profiles.

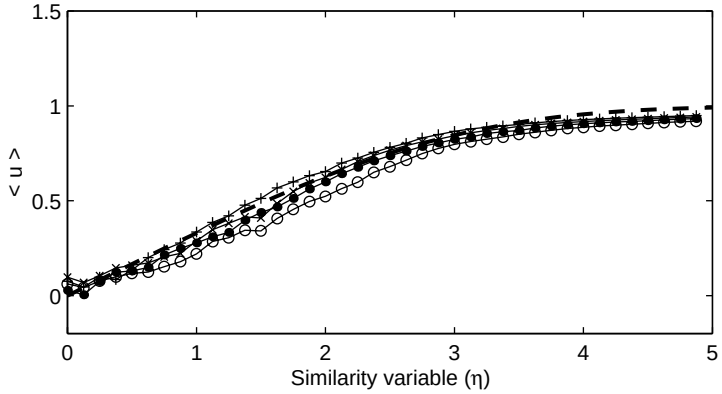

FIG. 5. Mean horizontal velocity profiles after step 50 averaged over preceding 47 steps at the four lateral locations indicated in Fig. 4; dashed line is the Blasius profile.

associated with Figs. 4 and 5 starts impulsively at $t = 0$; since the averaging process over the first three steps will be associated with impulsive transients, these steps are excluded from the averaging.

The prescription of (27) suggests that Blasius flow should correspond to a choice of sheet length l_I of order $1/Re$. This parameter can be varied; the "closeness" to Blasius profile (in an L^2 sense) can be examined for a choice of smoothing prescription. Figure 6a illustrates the result of choosing sheet lengths in the range $l_I \in [0.003, 0.01]$, with $\delta_I = l_I/2$, and with the average taken over 30 time-steps. We note a minimum in error in the neighborhood of the

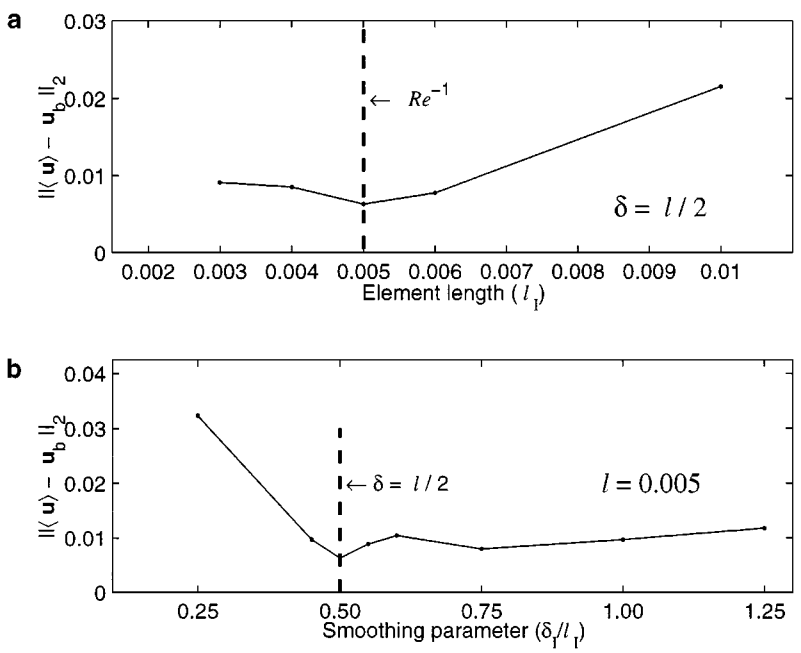

FIG. 6. (a) L^2 error norm expressing fit to Blasius profile of the aggregated four velocity profiles at lateral locations indicated in Fig. 4 as a function of sheet length l with smoothing parameters $\delta = l/2$; (b) L^2 error norm for $l = 0.005$ as a function of smoothing parameter, δ/l.

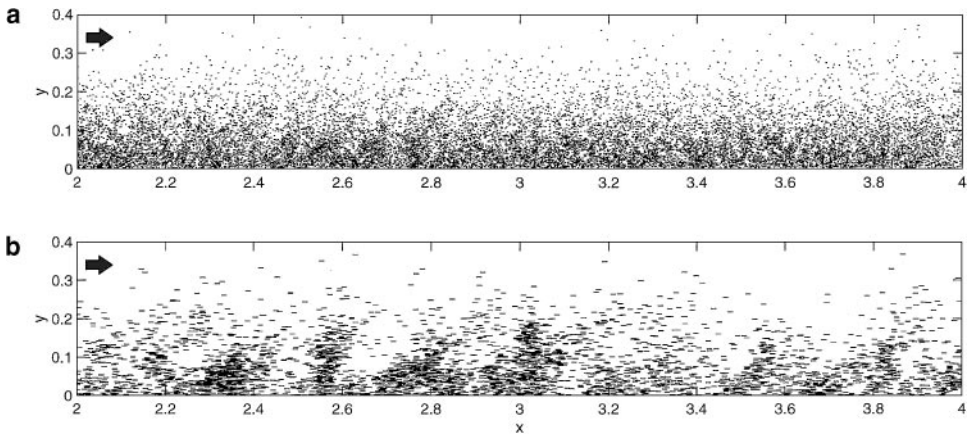

FIG. 7. Downstream distribution of vortex dipole sheets at two levels of spatial refinement. (a) $l_I = 0.003$; and (b) $l_I = 0.012$.

prescription (27). Figure 6b illustrates how error varies with smoothing parameter, for fixed sheet length ($l_I = 0.005$).

If we observe the distribution of dipole elements at increasing distance downstream, the velocity profiles become increasingly less self-similar. Downstream sections seem to achieve a stable quasi-uniform boundary layer thickness as time advances. Figure 7 illustrates the downstream distribution for $x \in [2, 4]$ for two choices of sheet length: $l_I = 0.003$ and $l_I = 0.012$. These choices correspond to parameters falling above or below the prescription defined by (27). In Fig. 7a we have $l_I < 1/Re$ and diffusion is expected to predominate over advection; in Fig. 7b we have $l_I > 1/Re$ and advection dominates. By construction, the scale of the parameter l_I expresses the spatial scale of impulse imparted to the flow; the evidence of Fig. 7 suggests that it also influences the scale of lateral structures which develop in the boundary layer.

7. FLOW PAST A CIRCULAR CYLINDER—CASE OF $\mathbf{m}_{II}$

7.1. Preliminary remarks. We investigate now the vorticity generation associated with flow past a bluff body related to the $\mathbf{m}_{II}$ decomposition in isolation.

We consider a circular cylinder, $\partial\mathcal{B}$, of unit radius centered at (0, 0). At time $t = 0$ a unit flow in the positive x-direction impinges on the body; unperturbed this flow is $U = (1, 0)$. At $t = 0$ (with no previously generated impulse or vorticity in the flow interior) the field $\mathbf{U}_{II} = (U_{II}, V_{II})$ can be determined consistent with condition (13) and with the uniform inlet/outlet condition of the free-stream. We have

$$U_{II} = 1 + \frac{x^2 - y^2}{r^4} \tag{28}$$

and

$$V_{II} = \frac{2xy}{r^4}. \tag{29}$$

Hence we can infer from (12) a normally oriented wall impulse associated with this free stream given by $\mathbf{m}_{II}^f \cdot \hat{\mathbf{r}} = -(U_{II}, V_{II}) \cdot \hat{\mathbf{r}}$, with $\hat{\mathbf{r}}$ the unit radial vector.

7.2. The field $\mathbf{u}_{II}$. In the case of the $\mathbf{m}_{II}$ decomposition we need to determine a field $\mathbf{u}_{II}$ consistent with condition (13) at each time-step.

One way to proceed is to express a perturbation velocity potential, Ψ^P, in terms of a single-layer potential function so that

$$\Psi^P(\mathbf{r}) = -\frac{1}{2\pi}\int_{\partial\mathcal{B}} \sigma(\mathbf{r}_o)\ln|\mathbf{r}-\mathbf{r}_o|\,dl(\mathbf{r}_o),$$

where $\sigma(\mathbf{r}_o)$ is a source distribution function at a point $\mathbf{r}_o$ on the cylinder $\partial\mathcal{B}$. From this we determine an perturbation velocity field, generally as

$$\mathbf{u}_{II}^P = \nabla^\perp\Psi^P = -\frac{1}{2\pi}\int_{\partial\mathcal{B}} \sigma(\mathbf{r}_o)\nabla^\perp\ln|\mathbf{r}-\mathbf{r}_o|\,dl(\mathbf{r}_o), \tag{30}$$

where $\nabla^\perp \equiv (-\partial/\partial y, \partial/\partial x)$. We identify $\mathbf{u}_{II}^P$ as the perturbation which, when added to the velocity associated with the field induced by the distribution of impulse ($\mathbf{u}_m$) achieves condition (13) on $\partial\mathcal{B}$. This is to say we write

$$\mathbf{u}_{II} = \mathbf{u}_m + \mathbf{u}_{II}^P \tag{31}$$

with $\mathbf{u}_{II}\cdot\mathbf{s} = 0$ on $\partial\mathcal{B}$. This leads to the integral equation developed by Martensen [21]

$$\frac{\sigma(\mathbf{r})}{2} + \frac{1}{2\pi}\int_{\partial\mathcal{B}} \sigma(\mathbf{r}_o)[-(y-y_o)s_x + (x-x_o)\,s_y]|\mathbf{r}-\mathbf{r}_o|^{-2}dl(\mathbf{r}_o) = \mathbf{u}_m\cdot\mathbf{s} \tag{32}$$

to be solved for σ at each point $\mathbf{r}\in\partial\mathcal{B}$, with $\mathbf{s} = (s_x, s_y)$ representing the local unit tangent vector at $\mathbf{r}$. This problem we can discretize, for example, using a constant-panel Nyström approach. Having solved for σ we deduce $\mathbf{u}_{II}^P$ everywhere in the fluid through a quadrature version of (30). Finally we determine the field, $\mathbf{u}_{II}$, from (31).

7.3. Creation and translation of vortex sheets. At points $\mathbf{x} = (x, y)$ on the cylinder, and at each time step, we require to determine the strength of the vortex sheet to be created there in order to establish impermeability. This strength derives from the lateral gradient of the normal component of velocity since $\kappa = -\xi d = \partial(\mathbf{u}_{II}\cdot\mathbf{n})/\partial s\, d$, where d is a vertical length scale which we may take to be some multiple of $\sqrt{1/Re}$.

We partition the circle $\partial\mathcal{B}$ into panels each of length l_{II}. At each time step the vorticity ξ is evaluated at the centroid of each panel using a difference approximation for the lateral velocity gradient. We will take the partition parameter l_{II} to be proportional to the viscous scale length—consistent with the discussion in Subsection 4.1. It is therefore to be scaled in inverse proportion to the square root of Reynolds number, i.e., $l_{II}\sim 1/\sqrt{Re}$.

At $t = 0$ a unit flow in the positive x-direction is incident on a unit circular cylinder centered at the origin (0, 0). As time progresses, thin vortex sheets are created at each time step on the cylinder's surface consistent with viscous boundary conditions. Apart from the distinct creation criteria, we have at this stage something which resembles a standard vortex method.

For flow induced by an ensemble of N vortex sheet elements $\{\kappa_j\}$, we can express the velocity as a Biot–Savart integral which takes a discretized form as described in Subsection 5.4. Since we require the field induced at a point (x, y) by an ensemble $\{\kappa_j\}$ located at points (x_j, y_j) in the flow interior to satisfy $\mathbf{u}\cdot\mathbf{n} = 0$ at $\partial\mathcal{B}$, we introduce a system of images $\{\kappa_j'\}$

of strength $\kappa'_j = -\kappa_j$ at inverse points $\mathbf{r}'_j = (r_j \cos\beta_j, r_j \sin\beta_j)$ inside the cylinder, where $\beta_j = \tan^{-1}(y_j/x_j)$ and $r_j^2 = x_j^2 + y_j^2$. In addition to these, to enforce irrotationality of the image field, an additional image is introduced at the center of the cylinder with strength $\sum_j \kappa_j$.

7.4. Numerical results. We illustrate the computation for the present case by pursuing the following numerical parameterization. We make a choice of time-step interval, dt, which is guided by the discussion in Section 2.4 of [24]. The free-stream velocity U can be varied relative to the dimensions of the cylinder in such a way that the product of U and dt is kept constant. We also keep the parameter $Re = Ur/\nu$ constant.

The fixed radius of the unit cylinder is $r = 1$. The cylinder surface is partitioned into 75 panels of length $2\pi/75$, corresponding to the intended sheet element length. Since a Poisson equation is to be solved over this surface, a second more refined partition is constructed for this purpose, with 500 nodes.

By way of demonstration we consider the flow illustrated in plate 94 in Van Dyke [11]: this represents a free-stream of 1.4 cm/s flowing past a cylinder of radius 0.5 cm; the Reynolds number is 140. We reflect this proportion between cylinder radius and free-stream velocity by the following model: we choose $U = 3$, $r = 1$, $Re = 140$. We determine $l_{II} = 2\pi/75 \simeq 1/\sqrt{Re}$. From the CFL condition we infer $dt = 0.02819$. The smoothing parameter is chosen to be $\delta = l_{II}/4$.

The flow is started impulsively at $t = 0$. At the initial time-step the free-stream field components described in Subsection 7.1, namely $\mathbf{U}_{II} = (U_{II}, V_{II})$, are calculated at the nodes of the refined partition; from this the radial component $\mathbf{m}_{II}^f \cdot \hat{\mathbf{r}}$ is inferred at each nodal point. Hence the lateral derivative $\partial(\mathbf{m}_{II}^f \cdot \hat{\mathbf{r}})/\partial s$ is calculated, with s the arc-length variable, taken positively in the direction of increasing angle (θ) measured from the positive x axis (i.e., from the downstream stagnation). This differentiation is achieved using center-differences. From this a vortex sheet strength κ is calculated.

Figure 8 illustrates the instantaneous distribution of sheet locations at 30-step intervals after impulsive start-up. At step 90 there are some 3200 elements represented in the flow.

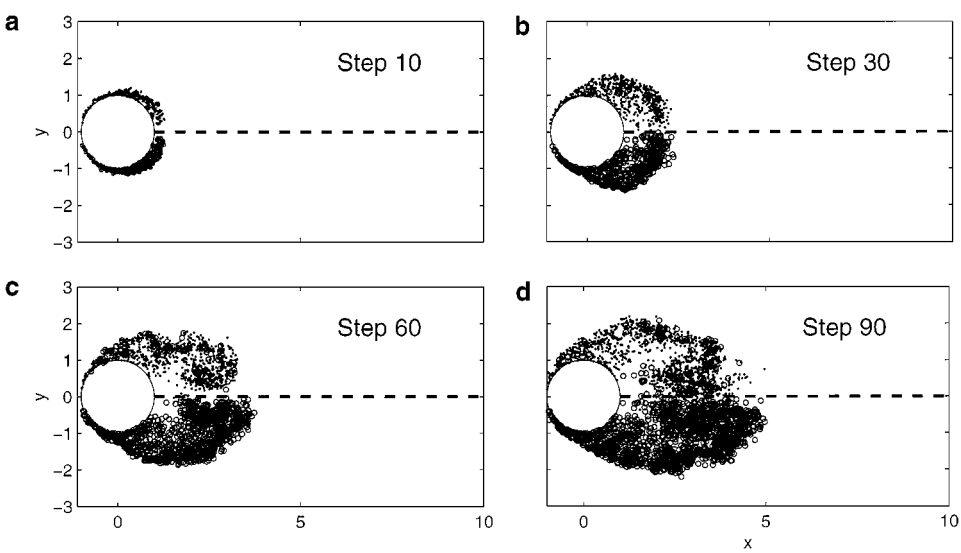

FIG. 8. Evolution from impulsive start-up of flow past a cylinder.

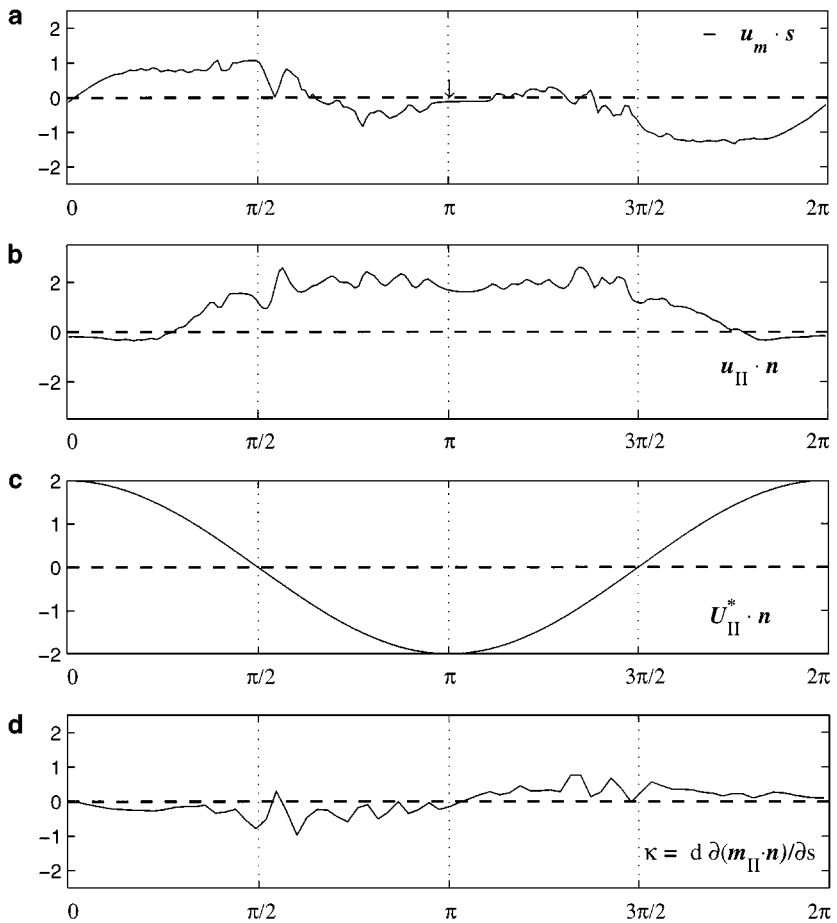

FIG. 9. Function distributions over the cylinder surface at step 90. (a) The right hand side to the integral equation (32); (b) normal component of field deduced from (32); (c) free-stream contribution defined in Subsection 7.1; (d) sheet strength κ (with $d = 0.25/\sqrt{Re}$).

The open circles represent elements whose sense is positive (i.e., induce a velocity which rotates counter clockwise). The filled circles indicate a negative sense. We note the structure of the wake begins to develop asymmetry at this step, and downstream oscillatory instability forms.

Figure 9 illustrates distributions (over the surface of the cylinder) of various functions which are relevant to the present calculation. These are plotted for the 90th time-step as a function of θ, the angle taken from the downstream stagnation. Figure 9a illustrates the distribution of tangential velocity induced by dipole elements (in the flow interior) created previously to the 90th time-step. This is namely $\mathbf{u}_m \cdot \mathbf{s}$, where $\mathbf{u}_m$ is the variable appearing on the right-hand side of the integral equation (32) and is the velocity field induced in $\mathbb{R}^3$ introduced in Subsection 3.2. (The downward arrow in Fig. 9a indicates the location of upstream stagnation on the cylinder, i.e., $\theta = \pi$.) Figure 9b illustrates the distribution of the field $\mathbf{u}_{II}$, determined from (31); this is a field normal to $\partial\mathcal{B}$. Figure 9c illustrates the component of the free-stream field $\mathbf{U}_{II}$, tangential to $\partial\mathcal{B}$; this is determined from (28) and

(29). The distribution of sheet-strength to be created at $\partial\mathcal{B}$ at the 90th time-step is illustrated in Fig. 9d. This is calculated from the lateral gradient (approximated by center-differences) of $\mathbf{m}_{II} \cdot \mathbf{n} = -(\mathbf{U}_{II} + \mathbf{u}_{II}) \cdot \mathbf{n}$.

Figures 10 and 11 illustrate the subsequent evolution of elements over 400 time-steps.

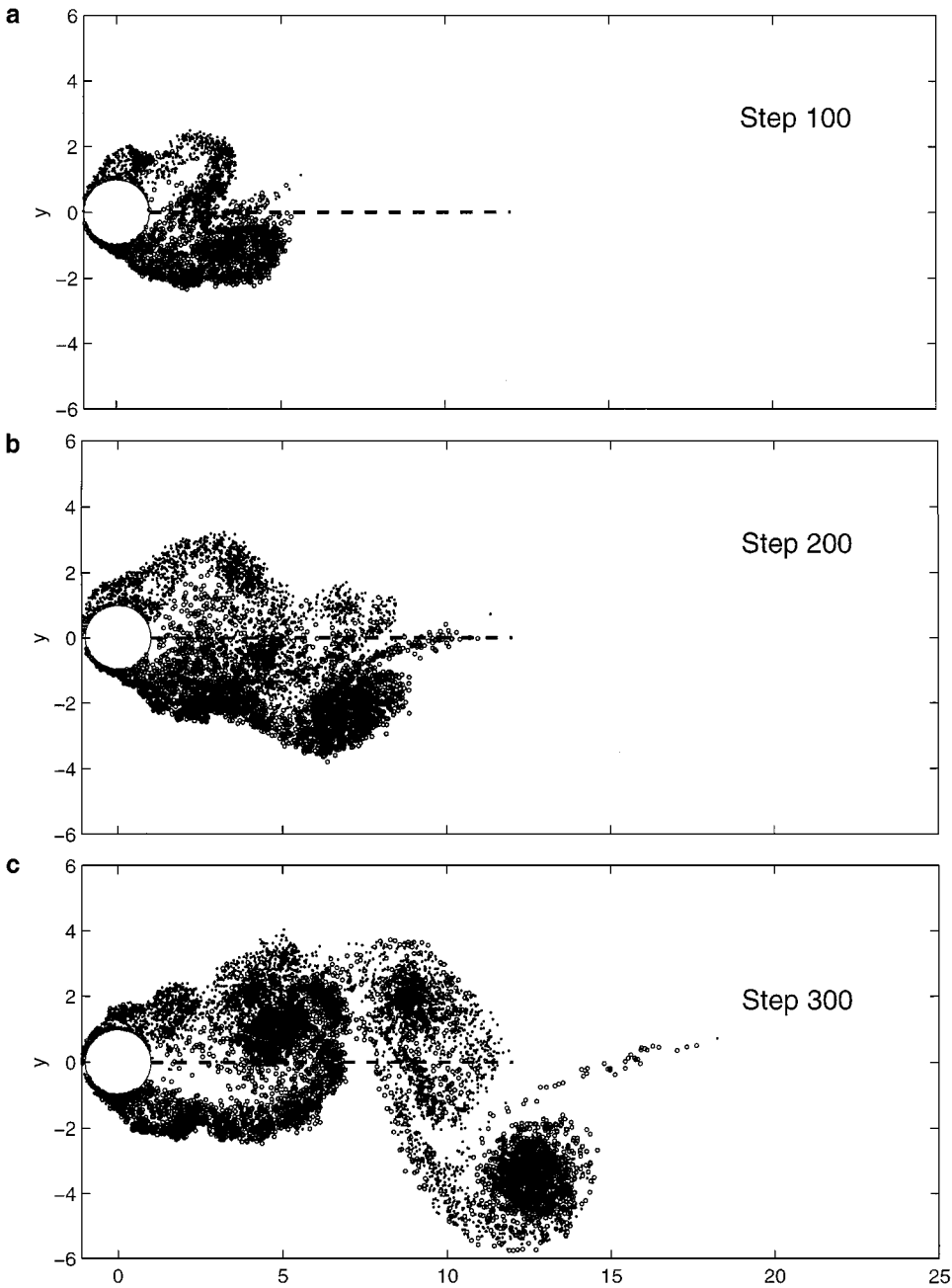

FIG. 10. Evolution of flow past a cylinder, $Re = 140$, $dt = 0.02819$, $U = 3.0$. Steps 100, 200, and 300.

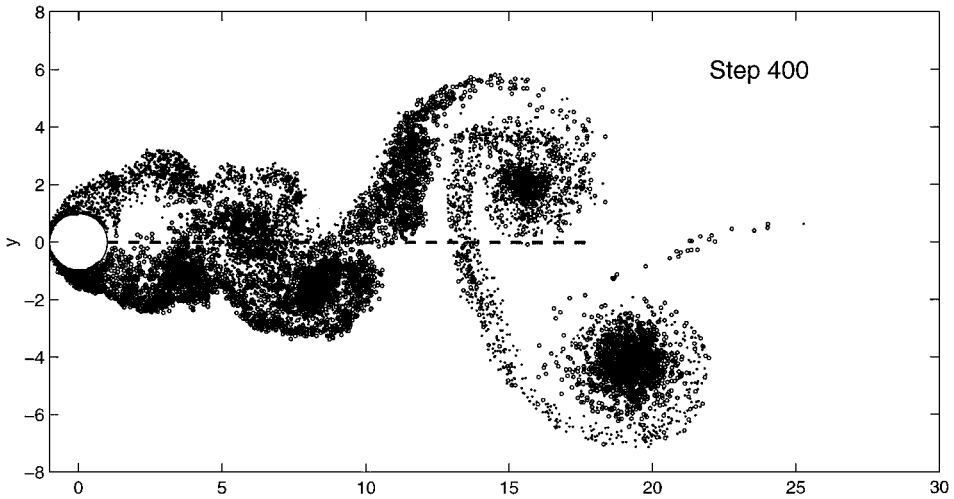

FIG. 11. Evolution of flow past a cylinder, step 400.

8. CONCLUSIONS

We have introduced two particular choices of the function ϕ in Eq. (2) which are consistent with wall impulse oriented in two orthogonal directions, normal and parallel to the wall, respectively. Each case can be related to the creation of impulse at the wall to effect the velocity boundary condition. Taking wall impulse density $\mathbf{m}$ to be normal to the wall is associated with the creation of vortex sheets; taking it to be parallel to the wall is associated with the creation of vortex dipole sheets. The two creation processes can, in principle, be superposed.

There has been experimental, numerical, and theoretical evidence to suggest that flow structures in wakes and in separating shear layers are somehow related to a combination of "single-sign vorticity" and "double-layer vortices" (roughly cast into present nomenclature: monopole sheets, and dipole sheets). See, for example, [1], or [16]. In an analysis of Euler flow, Moffatt [22] identifies the existence of two kinds of tangential discontinuity: that of velocity (vortex sheets) and that of vorticity (which in our language implies dipole sheets). The decompositions we propose provide a rationale for the creation of such objects at a wall based on the equation of motion and its associated wall boundary condition.

Our object here has been to introduce the idea of such decomposition and to illustrate this with numerical experiment. Our illustrations are constrained by obvious simplifying assumptions: for example, we use smoothing strategies which, while commonly invoked for vortex sheets [15, 1] nevertheless are not accompanied by a rigorous convergence theory. Also we do not express numerically the deformation and rotation of $\mathbf{m}_I$ elements in the present exercise.

Viewed as a method of "vorticity-creation," the decompositions presented here may seem counter-intuitive. Intuition in this matter is informed by the insights of Chorin [7] or Lighthill [19]—and originally Rosenhead [25] and Stokes (see [32, letter, Sect. 643])—who in various contexts consider surfaces of discontinuity in the flow as vortex sheets. A solid wall constitutes such a surface of discontinuity so it is plausible to associate a vortex sheet with a finite "slip" in velocity there. Consistent with this plausibility argument, the creation of single-layer (i.e., monopole) vortex sheets at a wall would be associated specifically with

the no-slip condition. However, a more complicated picture emerges from present impulse considerations. Vortex *dipole* sheets are created specifically to effect no-slip (that is to say $\mathbf{m}_I$ creation is associated with tangential impulse at the wall). Impulsive forces which develop normal to the wall determine the creation of $\mathbf{m}_{II}$ elements, these being equivalent, via their gradients, to the creation of *monopole* vortex sheets.

The $\mathbf{m}_{II}$ decomposition has an antecedence in the Lagrangian model of flow developed by Lord Kelvin (see [14]). Kelvin considers a stationary solid body immersed in a moving inviscid fluid (specifically in a velocity field with harmonic potential, equivalent to our irrotational $\mathbf{u}_{II}$ fields). The pressure exerted by the fluid normal to the surface of the body, integrated over an interval of time, is equated (with sign reversal) to the equilibriating impulse imparted to the fluid by the body. The $\mathbf{m}_I$ case can be seen as a complement to Kelvin's original model, one which generalizes it to include the tangential forces which preoccupied Stokes [28]. For $\mathbf{m}_I$-decomposition one conceives of a viscous shear stress tangential to the solid boundary. Integrated over a small interval of time, this is identified as that impulse imparted to the fluid by the action of wall friction.

There exists a three-dimensional analogue of the present impulse representation (discussed elsewhere—see [30]) which leads to the creation of elements which respect the solenoidality condition for vorticity. The creation principle does not, in itself, advance the global circulation of the flow.

The decomposition we describe would seem to be simple, reflecting the fact that it is a natural consequence of the Hodge decomposition (2). Yet there are promising indications that this simple decomposition may provide a basis for a dynamically complete Lagrangian representation of bounded viscous flow.

ACKNOWLEDGMENTS

The author thanks Alexandre Chorin for conversations over the years, and specifically for introducing the author to the impulse formulation. Raz Kupferman is also thanked for a discussion which proved particularly helpful.

REFERENCES

1. W. T. Ashurst and E. Meiburg, Three-dimensional shear layers via vortex dynamics, *J. Fluid Mech.* **189**, 87 (1988).
2. G. K. Batchelor, *An Introduction to Fluid Dynamics* (Cambridge Univ. Press, Cambridge, UK, 1967).
3. J. T. Beale and A. Majda, High order accurate vortex methods with explicit velocity kernels, *J. Comput. Phys.* **58**, 188 (1985).
4. P. S. Bernard, A deterministic vortex sheet method for boundary layer flow, *J. Comput. Phys.* **117**, 132 (1995).
5. T. F. Buttke, Lagrangian numerical methods which preserve the Hamiltonian structure of incompressible fluid flow, in *NASA ASI Series*, edited by J. T. Beale *et al.* (1993), Vol. 395, p. 301.
6. T. F. Buttke and A. J. Chorin, Turbulence calculations in magnetization variables, *Appl. Numer. Methods* **112**, 47 (1993).
7. A. J. Chorin, Vortex models and boundary layer instability, *SIAM J. Sci. Statist. Comput.* **1**, 1 (1980).
8. A. J. Chorin, *Computational Fluid Mechanics—Selected Papers* (Academic Press, New York, 1989).
9. R. Cortez, *Impulse-Based Methods for Fluid Flow*, Ph.D. thesis, Department of Mathematics, University of California, Berkeley, 1995.
10. R. Cortez, An impulse-based approximation of fluid motion due to boundary forces, *J. Comput. Phys.* **123**, 341 (1996).
11. M. Van Dyke, *An Album of Fluid Motion* (Parabolic Press, Stanford, 1988).

12. K. Gustafson and J. Sethian (Eds.), *Vortex Methods and Vortex Motion* (SIAM, Philadelphia, 1991).
13. J. D. Jackson, *Classical Electrodynamics* (Wiley, New York, 1975).
14. Sir William Thomson (Lord Kelvin), *Mathematical and Physical Papers* (Cambridge Univ. Press, Cambridge, UK, 1910), Vol. 4.
15. R. Krasny, Desingularization of periodic vortex sheet roll-up, *J. Comp.* **65**, 292 (1986).
16. R. Krasny, A vortex-dipole sheet model for a wake, *Phys. Fluids A* **1**, 173 (1989).
17. G. A. Kuz'min, Ideal incompressible hydrodynamics in terms of the vortex momentum density, *Phys. Lett. A* **96**, 88 (1983).
18. H. Lamb, *Hydrodynamics* (Cambridge, 1932).
19. M. J. Lighthill, Introduction, in *Laminar Boundary Layers*, edited by L. Rosenhead (Oxford Univ. Press, London, 1963).
20. J. Maddocks and R. Pego, An unconstrained Hamiltonian formulation for incompressible fluid flow, *Comm. Math. Phys.* **170**, 207 (1995).
21. E. Martensen, Berechnung der Drückverteilung an Gitterprofilen in ebener Potentialströmung mit einer Fredholmschen Integralgleichung, *Arch. Rational Mech. Anal.* **3**, 235 (1959).
22. H. K. Moffatt, Structure and stability of solutions of the Euler equations: A Lagrangian approach, *Phil. Trans. R. Soc. London. A* **333**, 321 (1990).
23. V. I. Oscledets, On a new way of writing the Navier–Stokes equation: The Hamiltonian formalism, *Russian Math. Surveys* **44**, 210 (1989).
24. E. G. Puckett, A study of the vortex sheet method and its rate of convergence, *J. Sci. Statist. Comput.* **10**, 298 (1989).
25. L. Rosenhead, Formation of vortices from a surface of discontinuity, *Proc. R. Soc. London A* **134**, 170 (1932).
26. G. Russo and P. Smereka, Impulse formulation of the Euler equations: General properties and numerical methods, *J. Fluid Mech.* **391**, 189 (1999).
27. G. Schwarz, *Hodge Decomposition—A method for Solving Boundary Value Problems*, Lecture Notes in Mathematics (Springer-Verlag, New York/Berlin, 1995), Vol. 1607.
28. Sir G. G. Stokes, *Mathematical and Physical Papers* (Cambridge Univ. Press, Cambridge, UK, 1880), Vol. 1.
29. D. M. Summers, A random vortex simulation of falkner-skan boundary layer flow, *J. Comput. Phys.* **85**, 86 (1989).
30. D. M. Summers and A. J. Chorin, Hybrid vortex/magnet methods for flow over a solid boundary, in *Vortex Flows and Related Numerical Methods, II*, edited by Y. Gagnon *et al.* (ESAIM, Proceedings, 1996), Vol. 1; http://www.emath.fr/proc/Vol.1/. p. 65.
31. D. M. Summers and A. J. Chorin, Numerical vorticity creation based on impulse conservation, *Proc. Nat. Acad. Sci. U.S.A.* **93**, 1881 (1996).
32. D. B. Wilson (Ed.), *The Correspondence between Sir George Gabriel Stokes and Sir William Thomson, Baron Kelvin of Largs* (Cambridge Univ. Press, Cambridge, UK, 1990).